ACS OMEGA

Open Access

http://pubs.acs.org/journal/acsodf

Article

High Removal Efficiency of Radioactive Iodine with In Situ-Synthesized Ag_2O−$Mg(OH)_2$ Plate Composites

Chunyang Zhang,* Le Zhang,* Bowen Zheng, Haoran Chu, Zhaofeng Liu, Yun Bai, Sicheng Chang, Song Yang, Ning Zhao, Qingshan Yang, and Yuheng Ma

Cite This: *ACS Omega* 2025, 10, 10251−10260

Read Online

ACCESS | Metrics & More | Article Recommendations | Supporting Information

ABSTRACT: To promote the capacity of adsorbing radioactive iodine (I^-) in acid and alkaline situations, a high-removal-efficiency adsorbent based on silver oxide (Ag_2O) and magnesium hydroxide ($Mg(OH)_2$) was synthesized by the in situ method. To determine the mechanism of this novel absorbent, batch experiments related to the temperature, pH, competitive ion (Cl^-), and kinetic analysis were carried out. The results showed that the Ag_2O−$Mg(OH)_2$ plate composites had high adsorption capacity and efficiency for I^- (409 mg/g, 25 °C) with a wide range of pH values (3−9). In addition, the adsorption time from the initial concentration to I^- removal (97.36%) was only 20 min. Competitive ion experiments depicted that Cl^- influenced the capacity of adsorbing I^-. The k value of the pseudo-second-order model and regression factor R^2 were 7.86 × 10^{-3}g mg^{-1} min^{-1} and 0.999 at 25 °C, respectively. The kinetics and XPS results proved that the mechanism of adsorption was chemical adsorption. Compared with other commercial adsorbents, the Ag_2O−$Mg(OH)_2$ plate composites had potential for application in nuclear wastewater treatment with low cost and high efficiency.

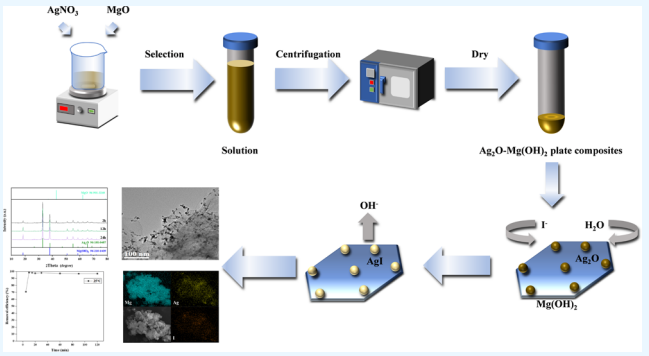

1. INTRODUCTION

Radioactive iodine, produced from human nuclear activities such as nuclear electricity generation and nuclear tests, can be easily dissolved in water.[1] Radioactive iodine mainly contains ^{129}I and ^{131}I, with corresponding half-lives of 1.57 × 10^7 years and 8 days, respectively.[2] ^{129}I stems from the circulation cooling water of the primary circuit, which would lead to long-term effects when leaked from the nuclear plant. Influences of the leakage accident in Fukushima (Japan) have been aggravated since the beginning of the discharge of radionuclides including radioactive iodine in 2023.[3] In addition, ^{131}I has been applied as nuclear medicine due to the thyroid's iodine-selective uptake ability.[4] Although its half-life is much shorter than that of ^{129}I, its higher radioactivity (1.5 × 10^{17} Bq) causes the risk of cancer, especially for doctors and patients.[5] Radioactive iodine has a high probability of causing harm to the human thyroid directly. Natural aquatic ecosystems can be polluted by radioactive iodine containing nuclear contaminated water, which has a potential influence on the health of people. Therefore, it is imminent to decrease radioactive iodine from wastewater.

Radioactive iodine can be removed by several methods including sorption,[6] ion exchange,[7] membrane separation,[8,9] and chemical precipitation.[10] Among them, sorption has been widely studied owing to its easier processes and lower costs. Activated carbon,[11,12] metal oxides,[13] and metal−organic frameworks (MOFs)[14−17] are the main adsorbents. However, the low adsorption capacity and low selectivity limit the application of activated carbon. Although MOFs exhibit great adsorption performance, their higher cost and poor stability have become limitations in a wide range of applications.[18] Metal oxides such as Ag_2O, bismuth oxide, and Cu_2O are potential materials to remove I^- attributed to their ability to adsorb iodine ions and form precipitates on the surface. Liu et al.[19] reported that bismuth oxide ($Bi_2O_{2.33}$) nanoparticles with a flower-like structure showed stability in both acid and alkaline environments and exhibited great selectivity among competitive anions. Zhang et al.[20] found that Bi_2O_3/LDHs with sponge-like porous structures can remove 94% of the initial I^- at near-neutral pH. Jiao et al.[21] obtained block Cu@Cu_2O, which reduced 96.65% of I^- in acid conditions with electrification.

Ag_2O is demonstrated as a significant ingredient for I^- adsorption, which can be precipitated more easily compared with Cl^-.[22] Thus, the reaction can generate a high removal

Received: October 24, 2024
Revised: February 19, 2025
Accepted: February 24, 2025
Published: March 5, 2025

efficiency in a short period.[23] Nevertheless, the removal ability is poor when Ag_2O has a low specific surface area. In addition, large particles of Ag_2O will lead to a reduction of the removal efficiency. Meanwhile, trace amounts of I^- make the sorption process difficult. Thus, the above problems can be resolved by choosing a support that has a substantial void ratio and a large specific surface area, anchoring target metal-oxide nanocrystals on its surface to obtain uniform dispersion.[24] Titanate,[2,25,26] natural minerals[27] and zeolites[28−31] are favorable materials that prevent the aggregation of Ag_2O, increasing its surface contact area are favorable materials that prevent aggregation of metal-oxide nanocrystals when increasing its surface contact area. Recently, silver-based materials fabricated by simplified chemical synthesis have gained considerable attention.[32] The literature shows that water-stable MOFs, zeolites, and cuprous oxide loading with Ag nanoparticles enhance the I^- removal efficiency.[33] However, higher costs and lower stability limit the application of these supports. Meanwhile, $Mg(OH)_2$ shows great economic advantages as a support for silver oxide nanoparticle loading. Most importantly, the $Mg(OH)_2$ support maintains its stability in high-radiation situations, and considerable research has been conducted on it. However, the aforementioned materials are limited due to the deactivation in strong acid and alkaline situations.[28] At present, there is an urgent need to seek a simplified synthesis process and low-cost way to overcome these problems.

In this study, we developed a new type of adsorbent with a high I^- removal efficiency, which has strong stability in a wide range of pH values by using only the stirring method at room temperature with $AgNO_3$ and MgO as precursors. Experiments are systematically implied with the following characteristics: reaction time, pH values, temperatures, and competitive ion (Cl^-). The adsorption mechanism and kinetic analysis were researched in detail.

2. MATERIALS AND METHODS

2.1. Materials. NaI was purchased from the Beichenfangzheng Chemical Reagent Factory, Tianjin, China. NaCl was purchased from Tianjin Zhiyuan Reagent Co., Tianjin, China. $AgNO_3$ was purchased from Sinopharm Chemical Reagent Co. Ltd, Shanghai, China. MgO was purchased from Bikeman Bio Co., Changde, China. $Mg(OH)_2$ was purchased from Damao Chemical Reagent Factory, Tianjin, China. These reagents were all of analytical grade purity and used as received without further purification. Also, nitric acid solution and NaOH (99% pure, Oubokai Chemical Engineering Co., Tianjin, China) were used to adjust the pH values of the solution. Experiments were all conducted with deionized water.

2.2. Synthesis of the Adsorbent. The synthesis process can be described as an in situ-synthesis. At room temperature, certain amounts of $AgNO_3$(2.94 mmol) and MgO (9.92 mmol) were added into deionized water (50.0 mL). Then, the solution was stirred with a magnetic rotor in a heating magnetic stirrer for 2 h. After stirring, the sediments were obtained through three cycles of centrifugation. The final precipitates were collected after drying at 60 °C for the whole night. For comparison, the same method was used to synthesize other samples with stirring periods of 12 and 24 h, respectively. Otherwise, single-phase Ag_2O was synthesized by the method described in the literature.[34] To compare with in situ-synthesis, Ag_2O and $Mg(OH)_2$ were mixed in a quartz mortar for 30 min directly to form composites.

2.3. Characterization. Crystalline structures of the adsorbents were characterized by using the powder X-ray diffraction (XRD) technique (DX2700, HAOYUAN INSTRUMENT, China). The diffractometer was equipped with copper target Kα, the scanning rate was 5°/min, and the scanning range was 10−80°. The phase composition and chemical state of the adsorbents before and after adsorption were determined by X-ray photoelectron spectroscopy (XPS) technology (Thermo SCIENTIFIC ESCALAB 250Xi, American). Field-emission scanning electron microscopy (FE-SEM, JEOL, JSM-7800F Prime, Japan; EDS, Thermo Scientific NORANTM System 7, American) and transmission electron microscopy (TEM, JEOL, JEM2100F, Japan) were performed to observe and analyze the micromorphology and composition of the samples. N_2 adsorption and desorption was performed by a porous physical adsorption instrument (QUANTACHROME, American), and the surface area was calculated by the Barrett−Emmett−Teller (BET) calculation.

2.4. Iodine Ion Removal Experiments. All experiments were conducted with nonradioactive iodine as a substitute to avoid the toxicity of radioactive iodine. A certain amount of iodine ion (10−100 mg_{NaI}/L) solution was prepared by dissolving NaI in 1 L of deionized water. A series of experiments were carried out with the mixture of 20 mg of adsorbent and 1 L of iodine solution in a beaker under a magnetic stirrer. The pH value was adjusted by NaOH and HNO_3 solutions. The effects of the equilibrium concentration of I^-, pH value, temperature, and competitive ions (Cl^-) on the removal rate of I^- were studied. Samples were taken from the solution through a needle and separated from the liquid−solid phase by a PES syringe filter. The residual concentration of I^- was determined by using a UV−Vis spectrophotometer (PE Company, Lambda750, American) at 226 nm. The coefficient of determination value R^2 calculated from the calibration line is 0.9987. The removal efficiencies were calculated according to the following three equations:

$$Q_t = \frac{C_i - C_t}{m} V \tag{1}$$

$$Q_e = \frac{C_i - C_e}{m} V \tag{2}$$

$$A_t = \frac{C_i - C_t}{C_i} \times 100\% \tag{3}$$

where C_i, C_e, and C_t are the concentrations of dissolved I^- (mg/L) initially, at equilibrium, and at time t, respectively. m is the weight of the adsorbent (g), and V is the volume of the solution (L). Q_t and Q_e are the amounts of I^- removed at time t and equilibrium, respectively. A_t is the removal efficiency at time t.

2.5. Adsorption Kinetics of the Adsorbent. The experiments of adsorption kinetics were conducted at room temperature in a neutral solution. 20 mg of adsorbent and 10 mg of NaI were added in 1 L of deionized water. Samples were taken from the solution at specific timepoints including 5, 10, 25, 20, 30, 60, 90, and 120 min. After filtration, the concentration of I^- was determined via UV−vis spectroscopy to calculate the Q_t of every sample according to eq 1. Considering further analysis of the behavior of the adsorbent in the iodine solution, the pseudo-first-order and pseudo-second-order models were applied to disclose the kinetics of adsorption. The first model was based on the physical

https://doi.org/10.1021/acsomega.4c09661
ACS Omega 2025, 10, 10251−10260

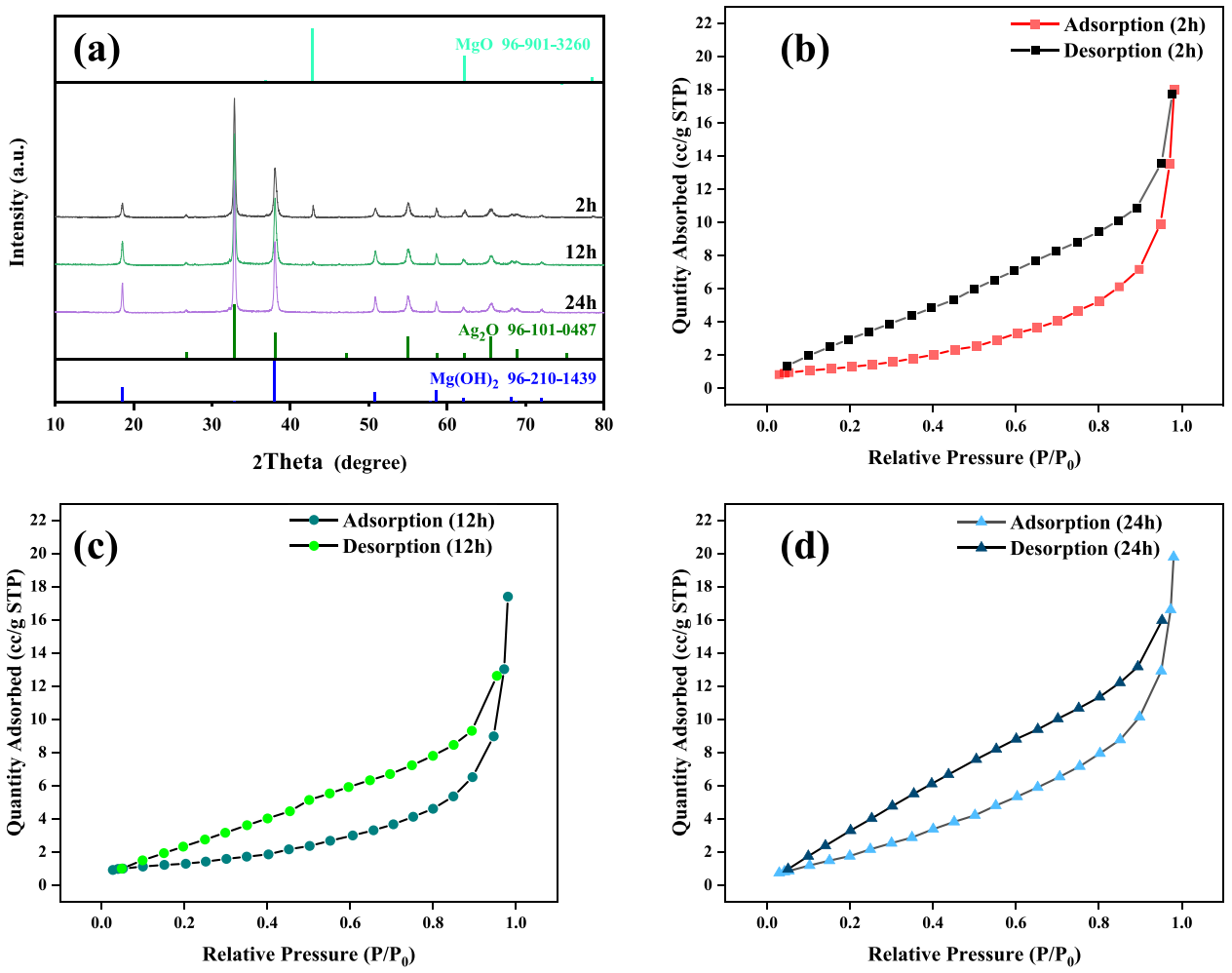

Figure 1. XRD patterns of the adsorbent with different times (a). N_2 adsorption and desorption isotherms of $Ag_2O-Mg(OH)_2$ plate composites with times of 2 h (b), 12 h (c), and 24 h (d).

absorption theory, while the other was chemisorption involving electron sharing and transfer between the adsorbent and adsorbate. The equations of linear expression of the pseudo-first-order and pseudo-second-order models were as follows:

$$\ln(Q_e - Q_t) = \ln Q_e - k_1 t \tag{4}$$

$$\frac{t}{Q_t} = \frac{1}{Q_e} t + \frac{1}{k_2 Q_e^{\,2}} \tag{5}$$

where k_1 and k_2 are constants that represent the first-order and second-order rate coefficients, respectively.

2.6. Determination of the Removal Efficiency in the Presence of Competitive Ions. To investigate the influence of competitive ions on the removal efficiency of I^-, 10 mg of NaI was put into 1 L of deionized water with a certain content of NaCl to obtain a solution for competitive experiments. The adsorbents were stirred with the solution for 20 min. Then, the residual content of iodine was determined by UV−vis spectroscopy.

3. RESULTS AND DISCUSSION

3.1. Phase Structure. To determine the phase structure of the adsorbent, the XRD patterns were measured. Figure 1 displays the XRD patterns and N_2 adsorption and desorption isotherm of the adsorbent under different synthesis times. As shown in Figure 1a, the highest intensity peak appeared at a distinct diffraction angle 2θ = 32.87°, corresponding to the interplanar phase of Ag_2O (1 1 1), indicating that Ag_2O was successfully formed during the stirring synthesis process. It can also be seen from Figure 1a that the diffraction peak of MgO gradually becomes weakened with the stirring time increasing, and the $Mg(OH)_2$ diffraction peak becomes stronger. At 24h, the diffraction peak of MgO disappeared, which indicated that the $Ag_2O-Mg(OH)_2$ composites were successfully synthesized. The results of N_2 adsorption and desorption experiments of $Ag_2O-Mg(OH)_2$ composites are shown in Figure 1b−d with synthesis times of 2, 12, and 24 h. According to the figures, all of these three samples showed type IV isotherms and H3 hysteresis loops, which suggested that mesoporous materials were obtained. The pore sizes of $Ag_2O-Mg(OH)_2$ composites were 3.432 nm (2 h), 3.430 nm (12 h), and 3.097 nm (24 h) by the BJH adsorption method, respectively. Theoretically, the smaller pore size and the larger BET surface area were beneficial to the adsorption property. Based on the XRD analysis, it can be concluded that the $Ag_2O-Mg(OH)_2$ composites were successfully synthesized at 24h. Thus, the following experiments would be conducted with the material synthesized at 24 h.

Figure 2 shows the microstructure and element mapping distribution of $Ag_2O-Mg(OH)_2$ composites. It can be seen

https://doi.org/10.1021/acsomega.4c09661
ACS Omega 2025, 10, 10251−10260

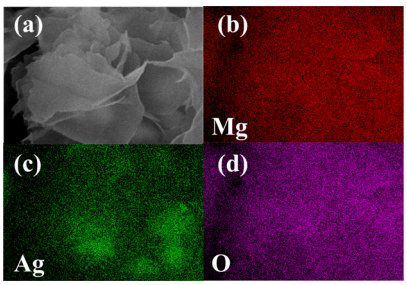

Figure 2. Microstructure and elemental mapping analyses of Ag_2O−$Mg(OH)_2$ plate composites before the reaction (a−d).

that Ag_2O−$Mg(OH)_2$ composites have plate-like structures. According to the literature,[35] this space construction was $Mg(OH)_2$, which was beneficial to form a mesoporous structure. To some extent, the plate-like structure promoted the dispersion of Ag_2O. The mapping results demonstrated that Ag_2O was dispersed on the $Mg(OH)_2$ plate uniformly. This phenomenon would encourage the adsorption of I^-. This clearly proved that the plate-like $Mg(OH)_2$ was an ideal carrier for Ag_2O. According to the analysis of Figure 1 and the literature,[35] the mesopores can be attributed to the fact that the MgO crystals were dissolved in water and hydroxylated into $Mg(OH)_2$ primary particles and then aggregated to produce large plate-like materials through oriented attachment.

Figure 3 shows the respective typical TEM images of the adsorbent. It can be seen that many nanoparticles were well-

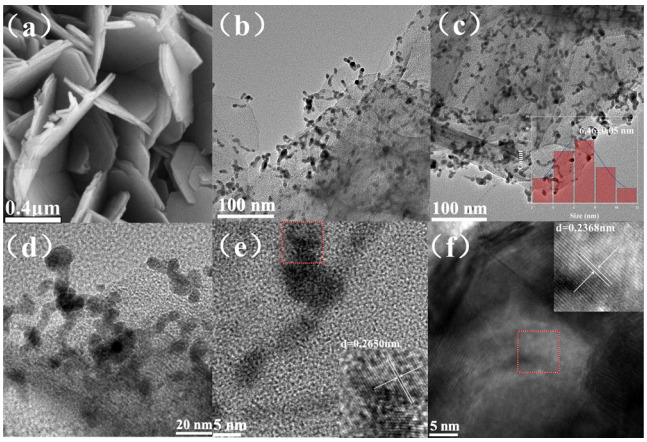

Figure 3. SEM image of Ag_2O−$Mg(OH)_2$ plate composites (a). TEM images of the adsorbent (b−d). Inset in (c): statistics of particle size distribution in (c) in 100 nm staff. Interplanar spacings of Ag_2O (e) and $Mg(OH)_2$ (f).

distributed on the plate. The nanoparticle size was about 6.46 ± 0.05 nm. The interplanar phases of the particles were 0.265 and 0.236 nm corresponding to the (1 1 1) plane of Ag_2O and (1 0 1) plane of $Mg(OH)_2$,[36,37] respectively. This clearly illustrates that Ag_2O nanoparticles were loaded on the $Mg(OH)_2$ plate successfully. Similarly, it is certain that the composites would be beneficial for NaI adsorption.

3.2. Properties of Ag_2O−$Mg(OH)_2$ Plate Composites.

Figure 4 shows the I^- removal efficiency of the Ag_2O−$Mg(OH)_2$ composites. Figure 4a shows that the synthesis temperature has a significant influence on the removal efficiency. With a higher synthesis temperature, the composites showed a lower removal efficiency. When the reaction temperature was 25 °C, the removal efficiency reached 97.36% of the initial concentration within 10 min, while the efficiency was only 65% at 45 °C. This result indicated that the optimal reaction adsorption temperature was 25 °C. However, the adsorption efficiency at the equilibrium of the three temperatures reached up to 97%, suggesting that the material has good thermal stability. According to the results above, considering that the time at which the adsorbent reached the equilibrium adsorption was 20 min, subsequent experiments would be conducted in the same time.

To investigate the influence of pH values at 25 °C, the results are shown in Figure 4b. It can be seen that the composites retained high removal efficiency over wide pH values (3−9). According to the literature,[38] this work shows a strategy in acid and alkaline conditions and can be used in practical applications. To be noticed, the pH values of the solution increased under acidic conditions, which may suggest that the composites had a certain buffer to acidic conditions. The increase in pH value can be attributed to the fact that the $Mg(OH)_2$ nanoplate participated in the reaction with hydrions more frequently due to its large specific surface area and alkalinity in acid situation. However, the pH value barely changed in the alkaline situation because the alkaline condition was beneficial to keep the $Mg(OH)_2$ nanoplate structure stable.

Considering the future application of the material to cope with complex aqueous situations, experiments were performed to explore the performance of the material mainly against chloride ions. Cl^-(NaCl) was used as a competitive ion. The result is depicted in Figure 4c. It can be seen that with a higher Cl^- concentration, the removal efficiency of I^- would decrease to 60% even at a concentration of 200 mg/L. This confirmed that the Ag_2O−$Mg(OH)_2$ plate composites had a certain anticompetitive ion ability.

Figure 4d shows the influence of the adsorbent concentration on the I^- removal efficiency. It can be seen that the removal efficiency was lower with an adsorbent content below 30 mg/L. However, with a high concentration of adsorbent, the removal efficiency of I^- was stable. Moreover, when the adsorbent content increased to 30 mg/L, the removal efficiency of I^- reached 90%, which effectively alleviated the influence of coprecipitation[39] between the target ions and competing ions. Then, the removal efficiency of I^- returned to a high performance as the adsorbent concentration continued to increase. These results proved that the method of increasing the adsorbent would be a response to a high concentration of Cl^- in the removal of I^-. Although the ability to absorb I^- was actually affected by Cl^-, considering the balance between the I^- removal efficiency and the cost of the adsorbent, the Ag_2O−$Mg(OH)_2$ plate composites can be suggested as an effective method. Thus, the concentration of 20 mg/L adsorbent was acceptable to remove I^-.

In practical applications, medical wastewater usually contains a high concentration of NaCl. In order to ensure that the adsorbent shows favorable performance, the concentration of NaCl was fixed as 100 mg/L. To determine the influence of the mass ratio between NaCl and NaI (Figure 4e), the concentration of I^- was increased to explore the adsorption capacity of the adsorbent (20 mg) under a fixed NaCl concentration (100 mg/L). With an increase in I^-, the adsorption saturation phenomenon occurred when the content of the adsorbent was fixed. The capacity of the saturation adsorption of I^- under interference was calculated. When the

https://doi.org/10.1021/acsomega.4c09661
ACS Omega 2025, 10, 10251−10260

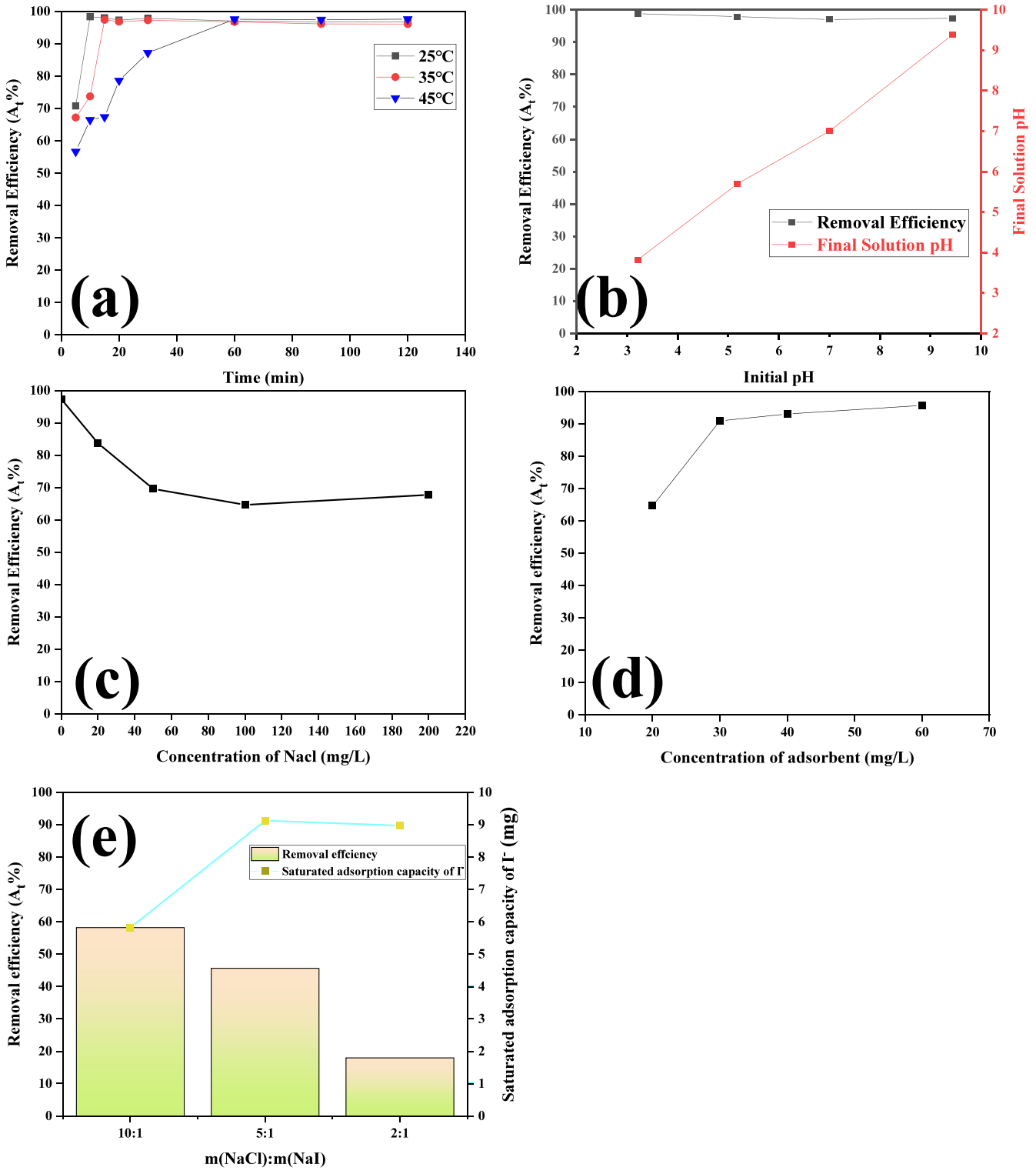

Figure 4. Removal efficiency of I^- by the Ag_2O−$Mg(OH)_2$ plate composite at different temperatures (a) and pH values (b). Removal efficiency of I^- in the presence of the competitive ion Cl^-(c). Effects of the adsorbent concentration on the I^- removal efficiency (d). Effects of I^-concentration on the I^- removal efficiency (e).

mass ratio changed from 10:1 to 2:1, the adsorption capacity first increased and then slightly decreased with increasing I^-. It can be inferred that the maximum saturation adsorption capacity was maintained at about 9 mg/L of NaI in the presence of a higher concentration of I^-. It is suggested that a higher concentration of I^- facilitated the adsorption capacity of I^-. To some extent, the removal efficiency of I^- by Ag_2O−$Mg(OH)_2$ plate composites would be affected by the presence of competitive ions (Cl^-).

3.3. Kinetics of Adsorption. Figure 5 shows the curves obtained by fitting two equations through calculations. Relevant statistics are also displayed in Table S1. The regression factor (R^2) values were all less than 0.900 under the pseudo-first-order kinetic equation and decreased with

https://doi.org/10.1021/acsomega.4c09661
ACS Omega 2025, 10, 10251−10260

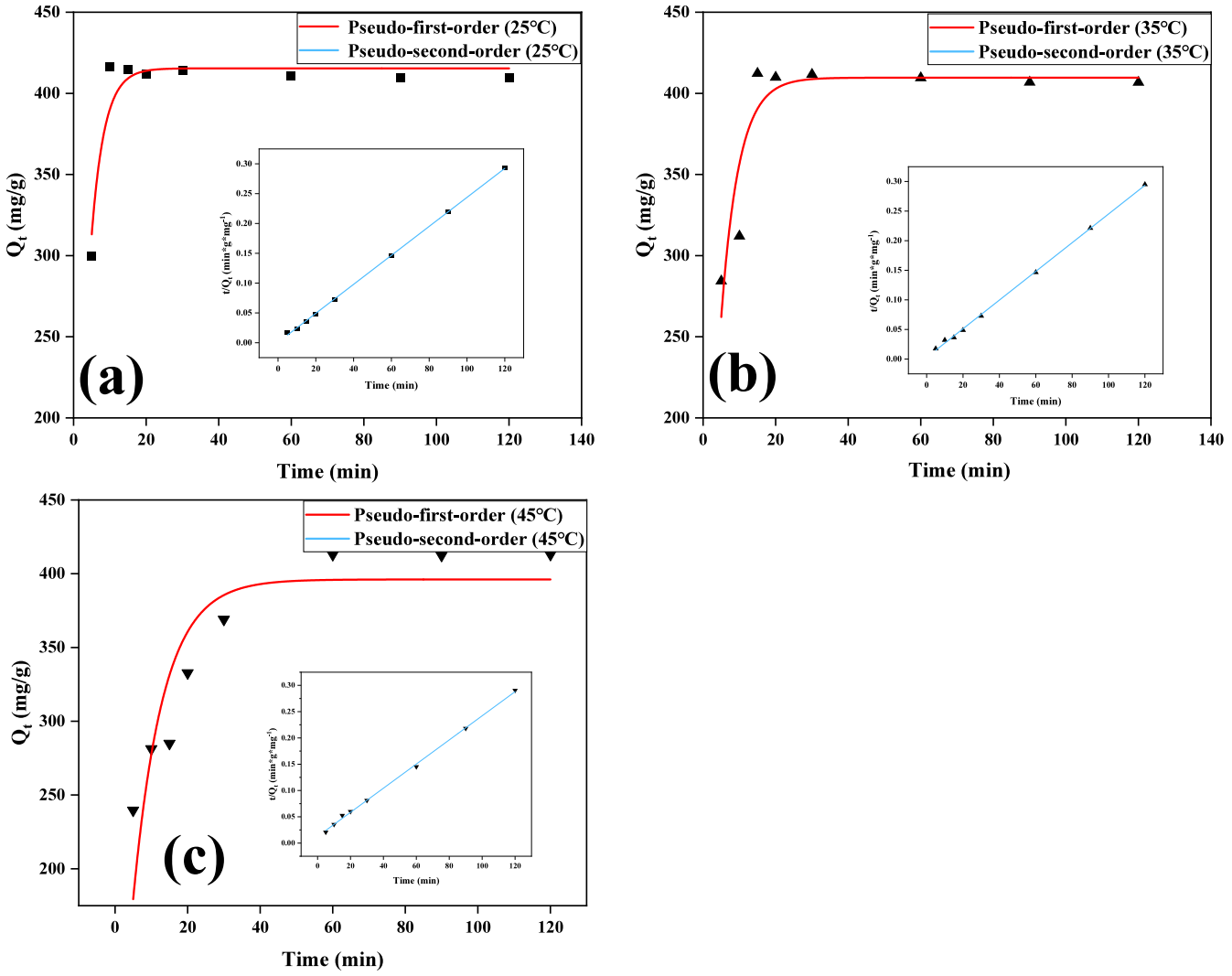

Figure 5. Adsorption kinetic curves of iodine by Ag_2O−$Mg(OH)_2$ plate composites at temperatures of 25 (a), 35 (b), and 45 °C (c).

increasing temperature. Fitting the pseudo-second-order kinetic equation, R^2 values reached 0.999 under all temperatures, which was closer to 1 than that of the pseudo-first-order kinetic equation. The I^- adsorption results obtained by experiments (Q_{exp}) were quite similar to that obtained by calculation (Q_{cal}). These results indicated that the Ag_2O−$Mg(OH)_2$ plate composites fit better with the pseudo-second-order kinetics. This also meant that the adsorption of I^- uniformly occurred at various adsorption sites on Ag_2O nanoparticles that were loaded on $Mg(OH)_2$ plates. Meanwhile, this phenomenon was also consistent with the TEM and SEM results. As discussed above, it can be considered that the adsorption process was chemisorption.

3.4. Adsorption Mechanism. After reaction with NaI, the element mapping results are displayed in Figure 6. Compared with Figure 2, the mapping of silver content decreased in a small range. However, the I element appeared, and the distribution of Ag and I elements highly coincided. This was also consistent with the analysis results of the kinetics. This demonstrated that AgI was formed in the process of contact and adsorbed on the surface of adsorbents. The fact that the morphology of the sample changed can be attributed to the fact that the composites used for characterization were collected after the reaction. The literature[40] shows that

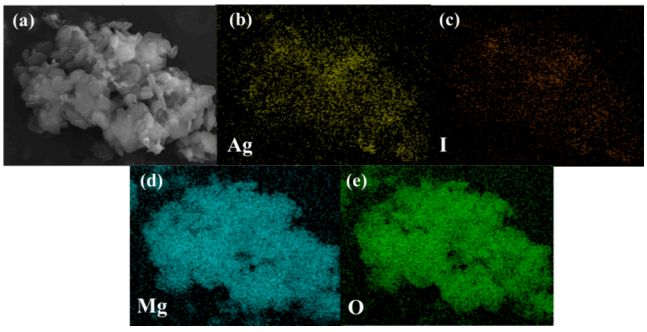

Figure 6. Elemental mapping analyses (a−d) and microstructure (e) of Ag_2O−$Mg(OH)_2$ plate composites after the reaction.

$Mg(OH)_2$ nanoplates may be dissolved in deionized water due to their solubility (9 mg/L) at 18 °C, and a higher temperature (25 °C) would aggravate the dissolution and result in shape change.

Surface analysis of Ag_2O−$Mg(OH)_2$ composites was carried out by XPS before and after the I^- reaction. As shown in Figure 7a, there were obviously different signals before and after the reaction. The I signal appeared after the reaction, which further demonstrated that I^- was successfully adsorbed

https://doi.org/10.1021/acsomega.4c09661
ACS Omega 2025, 10, 10251−10260

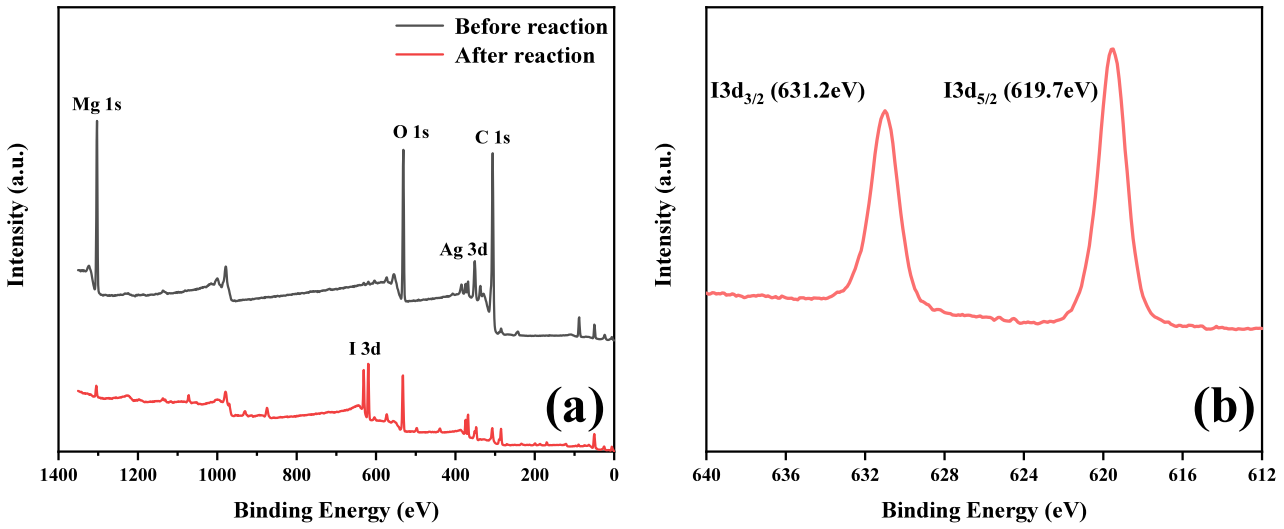

Figure 7. XPS spectra of Ag_2O−$Mg(OH)_2$ plate composites before and after iodine adsorption (a) and I 3d (b).

on the composites. According to Figure 7b, the shape analysis revealed that the peaks at 619.7 and 631.2 eV corresponded to I $3d_{3/2}$ and I $3d_{5/2}$ peaks of AgI,[41] respectively, indicating that the reaction process of Ag_2O−$Mg(OH)_2$ plate composites with NaI was a chemical adsorption reaction. The reaction equation of Ag_2O−$Mg(OH)_2$ plate composites and I^- can be described as below:

$$Ag_2O + 2I^- + H_2O = AgI + 2OH^- \quad (6)$$

To compare the performance of the composites synthesized by the ex situ method, Ag_2O and $Mg(OH)_2$ were ground in a quartz mortar at 25 °C for 30 min with a mass ratio of the two components identical to that used in the in situ method. Figure 8 shows the removal efficiencies of the two methods. As can be seen from Figure 8, the composites prepared by the ex situ method displayed a lower removal rate and lower removal efficiency even at a time of 120 min. The final adsorption efficiency was less than 60%, which confirmed that the ex situ method did not promote the capacity of the adsorbent. The ingredients of this adsorbent prepared by the ex situ method were used to conduct this experiment (Figure S1). SEM images of the ex situ ingredient materials are displayed in Figure S3. It can be seen that the synthesized Ag_2O spherical nanoparticles aggregated as shown in Figure S3a, which reduced their removal efficiency on I^-. Compared with the ex situ method, Ag_2O particles and $Mg(OH)_2$ nanoplates were observed by fitting together morphologically, as shown in Figure S3b. The TEM image of the ex situ-synthesized adsorbent further confirmed that Ag_2O particles cannot be anchored uniformly on the $Mg(OH)_2$ plate, which reduced its specific surface area and hindered the I^- removal ability. Hence, this confirmed that the in situ method had a high removal efficiency of I^-, and the composites had a wide potential for application in nuclear medical wastewater.

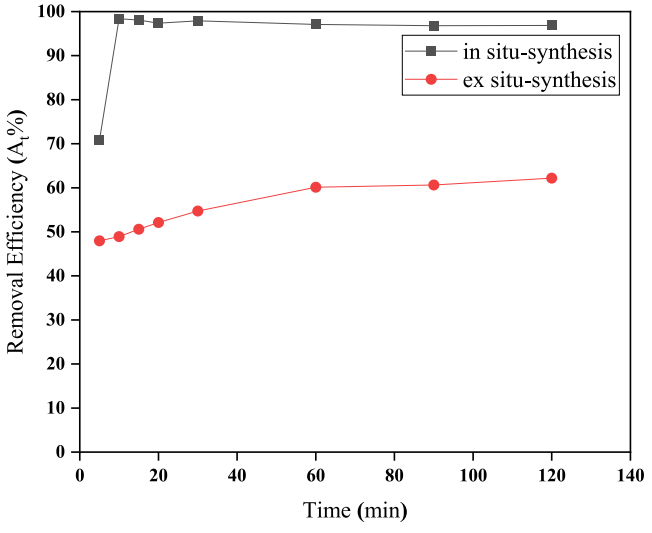

Figure 8. Removal efficiencies of the in situ and ex situ synthesis methods.

3.5. Cost Comparison of Ag_2O−$Mg(OH)_2$ Plate Composites. To evaluate the cost, the commercial adsorbents were compared with Ag_2O−$Mg(OH)_2$ plate composites. As can be seen from Figure S2, the composites had a much higher removal efficiency of I^- compared with activated carbon(AC), XAD-4 resin, and 251 × 8Cl resin. However, the 201 × 7Cl resin represented nearly the same efficiency in 24 h contact. Hence, aiming at the cost and efficiency of the 201 × 7Cl resin and Ag_2O−$Mg(OH)_2$ plate composites, further research was carried out. The cost comparison studies are shown in Table S2. It is clearly demonstrated that the Ag_2O−$Mg(OH)_2$ plate composites exhibited excellent performance and outstanding efficiency in I^- removal in the initial 60 min even with low adsorbent concentration (20 mg/L). The removal efficiency was 10 times higher than that of 201 × 7Cl resin (200 mg/L). Comprehensively, it is certain that the composites have the advantage of low cost for I^- removal and the potential for commercial application.

4. CONCLUSIONS

In this work, we successfully synthesized Ag_2O−$Mg(OH)_2$ plate composites through an in situ synthesis method. The TEM and SEM test results confirmed that Ag_2O nanoparticles were uniformly distributed on the surface of the $Mg(OH)_2$ plate. Due to the high selective absorption of Ag_2O and the large specific surface area of $Mg(OH)_2$, the adsorbent had a high removal efficiency for I^- (97.36%) during the adsorption process. The mechanism of the adsorbent was chemical

https://doi.org/10.1021/acsomega.4c09661
ACS Omega 2025, 10, 10251−10260

adsorption. Meanwhile, the composites maintained a high removal efficiency in a wide range of pH values (3−9) at room temperature. Compared with the ex situ-synthesized materials, the in situ synthesis process promoted the I^- removal performance. In conclusion, Ag_2O−$Mg(OH)_2$ plate composites can be used as candidate materials for nuclear medical wastewater treatment.

■ ASSOCIATED CONTENT

Supporting Information

The Supporting Information is available free of charge at https://pubs.acs.org/doi/10.1021/acsomega.4c09661.

Additional experimental details, comparison of adsorbents and simulated kinetic parameters (PDF)

■ AUTHOR INFORMATION

Corresponding Authors

Chunyang Zhang − *Department of Radioactive Waste Management, China Institute for Radiation Protection, Taiyuan 030006 Shanxi, P.R. China; Shanxi Provincial Engineering Research Center of Nuclear Facilities Decommissioning and Radioactive Waste Management, Taiyuan 030006 Shanxi, P.R. China;* orcid.org/0009-0005-0376-0456; Email: 18984342715@163.com

Le Zhang − *Department of Radioactive Waste Management, China Institute for Radiation Protection, Taiyuan 030006 Shanxi, P.R. China; Shanxi Provincial Engineering Research Center of Nuclear Facilities Decommissioning and Radioactive Waste Management, Taiyuan 030006 Shanxi, P.R. China*; Email: lezhang95@163.com

Authors

Bowen Zheng − *Department of Radioactive Waste Management, China Institute for Radiation Protection, Taiyuan 030006 Shanxi, P.R. China; Shanxi Provincial Engineering Research Center of Nuclear Facilities Decommissioning and Radioactive Waste Management, Taiyuan 030006 Shanxi, P.R. China*

Haoran Chu − *Department of Radioactive Waste Management, China Institute for Radiation Protection, Taiyuan 030006 Shanxi, P.R. China; Shanxi Provincial Engineering Research Center of Nuclear Facilities Decommissioning and Radioactive Waste Management, Taiyuan 030006 Shanxi, P.R. China*

Zhaofeng Liu − *Department of Radioactive Waste Management, China Institute for Radiation Protection, Taiyuan 030006 Shanxi, P.R. China; Shanxi Provincial Engineering Research Center of Nuclear Facilities Decommissioning and Radioactive Waste Management, Taiyuan 030006 Shanxi, P.R. China*

Yun Bai − *Department of Radioactive Waste Management, China Institute for Radiation Protection, Taiyuan 030006 Shanxi, P.R. China; Shanxi Provincial Engineering Research Center of Nuclear Facilities Decommissioning and Radioactive Waste Management, Taiyuan 030006 Shanxi, P.R. China*

Sicheng Chang − *Department of Radioactive Waste Management, China Institute for Radiation Protection, Taiyuan 030006 Shanxi, P.R. China; Shanxi Provincial Engineering Research Center of Nuclear Facilities Decommissioning and Radioactive Waste Management, Taiyuan 030006 Shanxi, P.R. China*

Song Yang − *Department of Radioactive Waste Management, China Institute for Radiation Protection, Taiyuan 030006 Shanxi, P.R. China; Shanxi Provincial Engineering Research Center of Nuclear Facilities Decommissioning and Radioactive Waste Management, Taiyuan 030006 Shanxi, P.R. China*

Ning Zhao − *Department of Radioactive Waste Management, China Institute for Radiation Protection, Taiyuan 030006 Shanxi, P.R. China; Shanxi Provincial Engineering Research Center of Nuclear Facilities Decommissioning and Radioactive Waste Management, Taiyuan 030006 Shanxi, P.R. China*

Qingshan Yang − *Department of Radioactive Waste Management, China Institute for Radiation Protection, Taiyuan 030006 Shanxi, P.R. China; Shanxi Provincial Engineering Research Center of Nuclear Facilities Decommissioning and Radioactive Waste Management, Taiyuan 030006 Shanxi, P.R. China*

Yuheng Ma − *Department of Radioactive Waste Management, China Institute for Radiation Protection, Taiyuan 030006 Shanxi, P.R. China; Shanxi Provincial Engineering Research Center of Nuclear Facilities Decommissioning and Radioactive Waste Management, Taiyuan 030006 Shanxi, P.R. China*

Complete contact information is available at: https://pubs.acs.org/10.1021/acsomega.4c09661

Author Contributions

C.Z. conducted the experiments, analyzed/collected the data, and wrote and revised the manuscript. L.Z. provided the idea and designed the experiments. B.Z. and Z.L. revised the manuscript. H.C. provided project support. Y.B., S.C., and S.Y. gave valuable advice to prepare the manuscript. N.Z., Q.Y., and Y.M. collected data. This manuscript was written through contributions of all authors. All authors have given approval to the final version of the manuscript.

Notes

The authors declare no competing financial interest.

■ ACKNOWLEDGMENTS

This work was supported by the National Natural Science Foundation of China (22206175).

■ REFERENCES

(1) Hou, X.; Hansen, V.; Aldahan, A.; Possnert, G.; Lind, O. C.; Lujaniene, G. A review on speciation of iodine-129 in the environmental and biological samples. *Anal. Chim. Acta* **2009**, *632* (2), 181−196.

(2) Bo, A.; Sarina, S.; Zheng, Z.; Yang, D.; Liu, H.; Zhu, H. Removal of radioactive iodine from water using Ag2O grafted titanate nanolamina as efficient adsorbent. *Journal of Hazardous Materials* **2013**, *246*−*247*, 199−205.

(3) Chang, Y.-C.; Zhao, X.; Han, Y. Responsibility under international law to prevent marine pollution from radioactive waste. *Ocean Coast. Manag.* **2022**, *227*, No. 106294.

(4) Shin, J. H.; Lee, S.-Y. Experiences of Korean patients with thyroid cancer receiving radioactive iodine therapy after total thyroidectomy. *Asia-Pacific Journal of Oncology Nursing* **2022**, *9* (3), 161−166.

(5) Wu, X.-Y.; Li, B.; Zhang, J.; Duan, L.-L.; Hu, B.-X.; Gao, Y.-J. Analysis of the clinical factors affecting excellent response of Iodine-131 treatment for pulmonary metastases from differentiated thyroid cancer. *Heliyon* **2023**, *9* (11), No. e20853.

(6) Moore, R. C.; Pearce, C. I.; Morad, J. W.; Chatterjee, S.; Levitskaia, T. G.; Asmussen, R. M.; Lawter, A. R.; Neeway, J. J.; Qafoku, N. P.; Rigali, M. J.; et al. Iodine immobilization by materials through sorption and redox-driven processes: A literature review. *Sci. Total Environ.* **2020**, *716*, 132820.
(7) Barton, D. N. T.; Robshaw, T. J.; Okusanya, O.; Kim, D.; Pepper, S. E.; Sharrad, C. A.; Lee, T. S.; Ogden, M. D. Remediation of radioiodine using polyamine anion exchange resins. *Journal of Industrial and Engineering Chemistry* **2019**, *78*, 210−221.
(8) Inoue, H.; Kagoshima, M.; Yamasaki, M.; Honda, Y. Radioactive iodine waste treatment using electrodialysis with an anion exchange paper membrane. *Applied Radiation and Isotopes* **2004**, *61* (6), 1189−1193.
(9) Lee, S.; Kim, Y.; Park, J.; Shon, H. K.; Hong, S. Treatment of medical radioactive liquid waste using Forward Osmosis (FO) membrane process. *J. Membr. Sci.* **2018**, *556*, 238−247.
(10) Iglesias, L.; Walther, C.; Medina, F.; Hölzer, A.; Neumann, A.; Lozano-Rodriguez, M. J.; Álvarez, M. G.; Torapava, N. A comprehensive study on iodine uptake by selected LDH phases via coprecipitation, anionic exchange and reconstruction. *Journal of Radioanalytical and Nuclear Chemistry* **2016**, *307* (1), 111−121.
(11) Zhang, X.; Yi, X.; Ouyang, J.; Wang, S.; Xu, D.; Qi, X.; Jiang, P.; Guo, X.; Wu, Y. Chitosan/carbon dots-loaded nanocellulose/layered double hydroxides composite hydrogel for effective detection and removal of iodide ion. *Chem. Eng. J.* **2024**, *479*, No. 147753.
(12) Sánchez-Polo, M.; Rivera-Utrilla, J.; Salhi, E.; von Gunten, U. Removal of bromide and iodide anions from drinking water by silver-activated carbon aerogels. *J. Colloid Interface Sci.* **2006**, *300* (1), 437−441.
(13) Zhang, M.; Liu, F.; Yang, H.; Xu, Z.; Wang, J.; Gong, Y. Elucidating the exceptional halide ion etching of bimetallic Ag−Cu oxides for efficient adsorption and porous nanostructure formation. *Materials Horizons* **2023**, *10* (7), 2506−2515.
(14) Gong, C.-H.; Li, Z.-Y.; Chen, K.-W.; Gu, A.-T.; Wang, P.; Yang, Y. Synthesis and characterization of Ag@Cu-based MOFs as efficient adsorbents for iodine anions removal from aqueous solutions. *J. Environ. Radioact.* **2023**, *265*, No. 107211.
(15) Garai, M.; Yavuz, C. T. Radioactive Strontium Removal from Seawater by a MOF via Two-Step Ion Exchange. *Chem.* **2019**, *5* (4), 750−752.
(16) Wang, T.; Zhao, H.; Zhao, X.; Liu, D. One-step preparation of Ag0-MOF composites for effective removal of iodide from water. *J. Solid State Chem.* **2022**, *305*, No. 122680.
(17) Zhong, X.-F.; Ma, Z.-C.; Lin, J.-J.; Wu, Y.; Liang, G.; Zhang, Y.-Y.; Chen, D.-J.; Xie, K.-P.; Mo, Z.-W.; Chen, X.-M. Metal−Organic Frameworks with Triazine and Amine Functional Groups for Iodine Removal and Sensitive Detection of Cu2+ and Fe3+ Ions. *Cryst. Growth Des.* **2023**, *23* (12), 8793−8799.
(18) Li, H.; Li, Y.; Li, B.; Liu, D.; Zhou, Y. Highly selective anchoring silver nanoclusters on MOF/SOF heterostructured framework for efficient adsorption of radioactive iodine from aqueous solution. *Chemosphere* **2020**, *252*, No. 126448.
(19) Liu, S.; Kang, S.; Wang, H.; Wang, G.; Zhao, H.; Cai, W. Nanosheets-built flowerlike micro/nanostructured Bi 2 O 2.33 and its highly efficient iodine removal performances. *Chemical Engineering Journal* **2016**, *289*, 219−230.
(20) Zhang, T.; Yue, X.; Gao, L.; Qiu, F.; Xu, J.; Rong, J.; Pan, J. Hierarchically porous bismuth oxide/layered double hydroxide composites: Preparation, characterization and iodine adsorption. *Journal of Cleaner Production* **2017**, *144*, 220−227.
(21) Jiao, H.; Li, Y.; Gao, K.; Zhao, J.; Wang, C.; Li, M.; Na, P. Efficient removal of radioactive iodide by three-dimensional Cu@Cu O: An adsorption and electrocatalytic oxidation coupling process. *Colloids Surf., A* **2020**, *602*, No. 124964.
(22) Chang, S.; Li, J.; Li, Y.; Chen, J.; Song, X.; Hou, J.; Qiu, D.; Zhang, X.; Zhang, Z.; Wang, R.; et al. Study on the microstructure and adsorption mechanism of different silver-based iodine adsorbents. *Inorg. Chim. Acta* **2024**, *569*, No. 122135.
(23) Zia, M. R.; Raza, M. A.; Park, S. H.; Irfan, N.; Ahmed, R.; Park, J. E.; Jeon, J.; Mushtaq, S. Removal of Radioactive Iodine Using Silver/Iron Oxide Composite Nanoadsorbents. *Nanomaterials* **2021**, *11* (3), 588.
(24) Feng, Y.; Yang, P.; Li, Y.; Gu, J. AgNPs-Containing Metal−Organic Frameworks for the Effective Adsorption and Immobilization of Radioactive Iodine. *Journal of Chemical & Engineering Data* **2020**, *65* (4), 1986−1992.
(25) Yang, D.; Liu, H.; Liu, L.; Sarina, S.; Zheng, Z.; Zhu, H. Silver oxide nanocrystals anchored on titanate nanotubes and nanofibers: promising candidates for entrapment of radioactive iodine anions. *Nanoscale* **2013**, *5* (22), 11011.
(26) Treushchenko, N. N.; Dmitrievskii, B. A.; Kazakov, A. A.; Tsvetkov, S. K.; Popov, A. Y.; Galkin, B. Y.; Treushchenko, V. A. Recovery and long-term storage of radioactive iodine using magnesium-containing composites. *Theoretical Foundations of Chemical Engineering* **2010**, *44* (4), 587−591.
(27) Kennedy, C. B.; Gault, A. G.; Fortin, D.; Clark, I. D.; Ferris, F. G. Retention of Iodide by Bacteriogenic Iron Oxides. *Geomicrobiology Journal* **2011**, *28* (5−6), 387−395.
(28) Tauanov, Z.; Inglezakis, V. J. Removal of iodide from water using silver nanoparticles-impregnated synthetic zeolites. *Science of The Total Environment* **2019**, *682*, 259−270.
(29) Ma, S.; Leung, K.-M.; Liao, C.; Chang, C.-K.; Zhou, Y.; Chen, S.; Zhao, X.; Zhao, Q.; Shih, K. Green conversion of waste alkaline battery material to zeolitic imidazolate framework-8 and its iodine capture mechanism. *J. Hazard. Mater.* **2024**, *469*, No. 133612.
(30) Warchoł, J.; Misaelides, P.; Petrus, R.; Zamboulis, D. Preparation and application of organo-modified zeolitic material in the removal of chromates and iodides. *Journal of Hazardous Materials* **2006**, *137* (3), 1410−1416.
(31) Cheng, M.; Luo, Y.; Geng, J.; Cui, R.; Qu, Y.; Sun, L.; Dou, Q.; Fu, H. Adsorption behavior of iodide ion by silver-doped zeolite 4A in LiCl-KCl molten salt. *Adv. Powder Technol.* **2022**, *33* (2), No. 103415.
(32) Zhao, X.; Han, X.; Li, Z.; Huang, H.; Liu, D.; Zhong, C. Enhanced removal of iodide from water induced by a metal-incorporated porous metal−organic framework. *Appl. Surf. Sci.* **2015**, *351*, 760−764.
(33) Tyupina, E. A.; Pryadko, A. V. Use of silver-containing sorbents in anionic species of radioactive iodine management in nuclear industry and the methods of obtaining them. *Journal of Radioanalytical and Nuclear Chemistry* **2024**, *333* (2), 599−613.
(34) Sullivan, K. T.; Wu, C.; Piekiel, N. W.; Gaskell, K.; Zachariah, M. R. Synthesis and reactivity of nano-Ag2O as an oxidizer for energetic systems yielding antimicrobial products. *Combust. Flame* **2013**, *160* (2), 438−446.
(35) Yu, J. C.; Xu, A. W.; Zhang, L.; Song, R.-Q.; Wu, L. Synthesis and Characterization of Porous Magnesium Hydroxide and Oxide Nanoplates. *J. Phys. Chem. B* **2004**, *108*, 64−70.
(36) Sarkar, D.; Ghosh, C. K.; Mukherjee, S.; Chattopadhyay, K. K. Three Dimensional Ag2O/TiO2 Type-II (p−n) Nanoheterojunctions for Superior Photocatalytic Activity. *ACS Appl. Mater. Interfaces* **2013**, *5* (2), 331−337.
(37) Das, P. S.; Dey, A.; Mandal, A. K.; Dey, N.; Mukhopadhyay, A. K. Synthesis of Mg(OH)2 micro/nano flowers at room temperature. *Journal of Advanced Ceramics* **2013**, *2* (2), 173−179.
(38) Jeong, H.; Lee, D. W.; Hong, S. J.; Kim, J.; Kim, M.; Kim, J.; Lee, H. S.; Park, T.-H.; Kim, H.-K.; Park, J. I.; et al. Selective removal of radioactive iodine from water using reusable Fe@Pt adsorbents. *Water Res.* **2022**, *222*, No. 118864.
(39) Lima, E. R. A.; Boström, M.; Horinek, D.; Biscaia, E. C.; Kunz, W.; Tavares, F. W. Co-Ion and Ion Competition Effects: Ion Distributions Close to a Hydrophobic Solid Surface in Mixed Electrolyte Solutions. *Langmuir* **2008**, *24* (8), 3944−3948.
(40) Pannach, M.; Bette, S.; Freyer, D. Solubility Equilibria in the System Mg(OH)2−MgCl2−H2O from 298 to 393 K. *Journal of Chemical & Engineering Data* **2017**, *62* (4), 1384−1396.
(41) Yang, M.; Pu, Y.; Wang, W.; Li, J.; Guo, X.; Shi, R.; Shi, Y. Highly efficient Ag2O/AgNbO3 p-n heterojunction photocatalysts

https://doi.org/10.1021/acsomega.4c09661
ACS Omega 2025, 10, 10251−10260

with enhanced visible-light responsive activity. *J. Alloys Compd.* **2019**, *811*, No. 151831.

https://doi.org/10.1021/acsomega.4c09661
ACS Omega 2025, 10, 10251−10260